IRIS AperTO

UNIVERSITÀ DEGLI STUDI DI TORINO

AperTO - Archivio Istituzionale Open Access dell'Università di Torino

Surface and Bulk Distribution of Fluorides and Ti3+ Species in TiO2 Nanosheets: Implications on Charge Carrier Dynamics and Photocatalysis

This is the author's manuscript

Original Citation:

Availability:

This version is available http://hdl.handle.net/2318/1743958 since 2020-07-27T15:18:52Z

Published version:

DOI:10.1021/acs.jpcc.9b10912

Terms of use:

Open Access

Anyone can freely access the full text of works made available as "Open Access". Works made available under a Creative Commons license can be used according to the terms and conditions of said license. Use of all other works requires consent of the right holder (author or publisher) if not exempted from copyright protection by the applicable law.

(Article begins on next page)

24 April 2024

Surface and Bulk Distribution of Fluorides and Ti^{3+} species in TiO_2 Nanosheets: Implications on Charge Carriers Dynamics and Photocatalysis

Francesco Pellegrino[a], Elena Morra[a], Lorenzo Mino[a], Gianmario Martra[a], Mario Chiesa[a]*, Valter Maurino[a]

a) Chemistry Department and NIS Inter-departmental Centre, University of Torino, Via P. Giuria 7, Torino, 10125, Italy

ABSTRACT. The effect on the reactivity and the kinetic of photogenerated e^-- h^+ pairs induced by post-synthesis treatments on shape controlled TiO_2 anatase nanosheets with dominant {001} facets are reported. Anatase nanosheets were prepared under hydrothermal conditions in the presence of fluoride ions as shape controllers. Fluorides were removed from the surface by washing with NaOH 0.1 M or by thermal treatment at 873 K. The effect of the progressive removal of fluorides on the electronic properties of the samples was monitored by EPR and UV-Vis-NIR-MIR spectroscopies, clearly separating the contributions of surface and bulk Ti^{3+} sites. The charge carrier dynamic was studied by EPR and photoelectrochemical measurements. These two complementary techniques provide insight into the recombination kinetics of the photogenerated carriers highlighting the role of both surface chemistry (F^- vs OH^- coverage) and morphology. The results indicate that the photocatalytic activity of TiO_2 anatase nanosheets could be controlled using different post-synthesis treatments. Electrochemical measurements revealed that the removal of surface fluorides leads to an increase of the photogenerated charge carriers' total depletion rate, whereas EPR experiments showed that the interfacial charge transfer to O_2 and H_2 is favored. As a result, the increase in carrier total depletion rate is due mainly to the increase of the interfacial charge transfer rate leading in turn to an increase of the photoreactivity, as witnessed by NO photo-oxidation.

INTRODUCTION

Crystal facet engineering of TiO_2 semiconductors nanoparticles (NPs) has an important role in surface reactivity optimization.[1] Through the rigorous control of surface chemistry and morphology the physicochemical properties of TiO_2 NPs can be modified in a controlled way, tuning these systems for a number of different applications in chemistry and materials sciences.[2] In the case of anatase the truncated tetragonal bi-pyramid, exposing predominantly {101} surfaces, is the equilibrium shape predicted by the Wulff construction. In 2008, the pioneering work of Yang *et al*. paved the way for new studies on the synthesis of anatase nano-sheets that largely expose the minority basal {001} surfaces.[3] The synthesis of TiO_2 nanosheets requires the use of capping agents able to decrease the surface energy. Fluoride ions are preferentially adsorbed on the {001} facets and act as shape controller increasing the occurrence of these otherwise high energy surfaces.[4-6] Ohno et al. reported that anatase {001} facets are privileged sites for the anodic processes, while {101} facets act as the reducing sites. These different characteristics are due to the presence of different surface energy levels onto different surfaces.[7-11] The difference in the energy levels drives electrons and holes to different anatase crystal facets, favouring the charge separation and leading to the so-called "surface heterojunction".[11-14]

In this context, two aspects can affect the photochemistry of the anatase nanosheets: surface termination and bulk doping. Indeed, bulk doping is one of the most employed strategies adopted in order to sensitize the absorption of TiO_2 nanoparticles in the visible range.[2, 15] The generation of intra-bandgap states modify the electronic structure of the material and, in turn, its reactivity.[16] The introduction of substitutional fluorine results in the formation of a lattice Ti^{3+} species where the excess unpaired electron is highly localized in the titanium 3d shell through a polaronic distortion. The mechanism is based on the so-called of valence induction and the stoichiometry of the solid can be represented as $Ti^{4+}_{(1-x)}$ Ti^{3+}_x $O^{2-}_{(2-x)}$ F^-_x.[17] Moreover, the surface interaction with donor and acceptor molecules (e.g. organic pollutants and oxygen) with the TiO_2 nanoparticles is influenced by the presence of adsorbate species introduced during the synthesis. For example, fluorides adsorbed on the TiO_2 surface strongly affect the interfacial hole and electron transfer in photocatalysis, as well as the interaction with water,[8] and the adsorption of substrates and O_2.[18] This, in turn, affects the photocatalytic activity by changing the

rates and mechanism of substrate oxidation,[19-20] as well as the rate of O_2 reduction and carrier recombination.[21] The post-synthesis treatments are usually undertaken to eliminate the residuals from the synthetic procedure. In a previous work,[22] a detailed characterization of formally {001} surface exposing TiO_2 nanosheets after different post synthesis treatments was performed. Specifically, the selective removal of surface localized fluorides from the nanoparticles' surface was obtained by F^-/OH^- exchange in NaOH 0.1 M, while the complete removal of fluorides, also from the bulk was obtained by thermal treatment at 873 K.[22] In the latter case, a (1×4) reconstruction of {001} facets likely occurred. Changes in surface properties with respect to pristine TiO_2 nanosheets were related to differences in photocatalytic performances, in terms of phenol photodegradation. Specifically, surface hydroxylation and hydration, that increased after F^-/OH^- exchange and decreased after calcination at 873 K. In this work complementary aspects relevant to the understanding of the photocatalytic mechanism are investigated by a multi-technique approach. EPR, UV-Vis-NIR-MIR and photoelectrochemical techniques are combined to evaluate bulk and surface electronic structures of TiO_2 anatase nanosheets, revealing the nature of their active sites and the behavior of the photogenerated charge carriers.

EXPERIMENTAL SECTION

Synthesis and Characterization of the materials.[22] The synthesis of TiO_2 nano-sheets was carried out with a solvothermal method following an established literature procedure.[23-24] In a typical synthesis, $Ti(OBu)_4$ (Aldrich reagent grade 97%) was poured into a Teflon lined stainless steel reactor and concentrated hydrofluoric acid (Aldrich reagent grade 47%) was added dropwise under stirring. The reactor was sealed and kept under stirring at 523 K for 24 hours. The obtained material was centrifuged and washed with acetone to remove the residual organics and then with water (Milli-Q). The aqueous suspensions are freeze-dried obtaining a bluish powder, due to the F^- doping of the anatase. This material exposes nearly 20% of the surface {101}. The as-synthesized material (n-sh) was washed with NaOH 0.1 M (2 hours under stirring at room temperature) to remove the fluorides from the surface. The Na^+ ions present at the surface of the nanoparticles were then removed washing with HNO_3 0.1 M and ultrapure water (MilliQ, Millipore). This material exposes nearly 20% of the surface {101}. The complete removal of the fluorides from the nanoparticles (bulk and surface), the as-synthesized material (n-sh) was heated at 873 K for 1 hour in air atmosphere (with a ramp of 6 K min^{-1}). The resulting powder is white. The fluoride removal was confirmed by chemical analysis. This material exposes nearly 40% of the surface {101}, due to the calcination treatment that induces a coalescence of the nanoparticles along the c-axis.

EPR measurements. X-band CW-EPR spectra were detected on a Bruker EMX spectrometer (MW frequency ~9.75 GHz) equipped with a cylindrical cavity. A modulation frequency of 100 kHz, a modulation amplitude of 0.2 mT and a microwave power of 0.1 mW were used. Pulse EPR experiments were performed on an ELEXYS 580 Bruker spectrometer operating at X-band (MW frequency 9.4 GHz), equipped with a liquid-helium cryostat from Oxford Inc. The magnetic field was measured by means of a Bruker ER035 M NMR gauss meter. Electron-spin-echo (ESE) detected EPR spectra were recorded with the Hahn echo sequence $\pi/2-\tau-\pi-\tau-$ echo. Microwave pulse lengths $t_{\pi/2}$ = 16 ns, t_π = 32 ns, and a shot repetition rate of 0.5 kHz were used. Two-pulses electron-spin-echo envelop modulation (2P-ESEEM) experiments were carried out with the Hahn echo pulse sequence, in which the τ value was incremented in steps of 8 ns starting from 100 ns. The time traces of the 2P-ESEEM spectra were baseline corrected, apodized with a Hamming window and zero filled; after two-dimensional Fourier transformation, the absolute value spectra were calculated. The quantification of the amount of EPR-active Ti^{3+} centres in the samples was performed employing as a reference Ti^{3+} standard solutions obtained dissolving the Tris(2,2,6,6-tetramethyl-3,5-heptanedionato)titanium(III) ($Ti(tmhd)_3$) complex in anhydrous toluene at five different molar concentrations in the range 2 - 20 mM. The standard solutions were prepared operating in glove-box. The EPR spectra of the standard frozen solutions were recorded under the same experimental conditions used for the samples (the microwave power was selected in order to avoid saturation effects of both the standard and the samples).

UV-Vis-NIR-MIR spectroscopy. UV-Vis-NIR spectra were recorded in diffuse reflectance mode on TiO_2 thick self-supported pellets with a Cary 5000 Varian spectrophotometer equipped with an integrating sphere with an inner coating of Spectralon®. This material was used also as reference. Mid-infrared (MIR) spectra were acquired using a Bruker IFS 66 FTIR spectrometer equipped with a Spectra Tech DRIFT accessory (model 0030-011) and a MCT detector. Each spectrum was collected in diffuse reflectance mode by averaging 128 interferograms at 4 cm^{-1} spectral resolution.

Electrochemical measurements. The electrochemical measurements were performed using a standard photo-electrochemical setup, composed of a computer-controlled potentiostat, AUTOLAB PGSTAT12, and a fluorescent source with λ_{max} = 365 nm (Philips PL-S 9W BLB, integrated irradiance = 20 W m^{-2}). The electrochemical cell was a conventional three-electrode cell with a 1 mm thick fused silica window. The counter and reference electrodes were a Glassy Carbon and a Ag/AgCl/KCl (3M) electrode, respectively. Both CV and OCP measurements were carried out under a N_2 atmosphere (flux 100 mL min^{-1}); also the solution (0.1 M KNO_3 as electrolyte, pH 6.5) was purged with N_2 for 20 min before each measurement in order to eliminate the residual O_2 present in the solution, to

obtain the recombination rate of the photogenerated carriers.

Photocatalytic Degradation of Nitric Oxide. The photocatalytic tests were carried out using a purposely designed reactor,[25-26] equipped with NO, NO_2, CO and VOC sensors (PID). The internal volume of the reactor is 15 ml, so a short time (10-30 s) is necessary for the stationary state. The humidity and temperature inside the reactor are continuously monitored, as well as the irradiation. The reaction gas mixture at proper concentrations was prepared using a Entech dynamic diluter model 4460. Total flux 0.5 l/min. The gas mixture enters the reaction chamber where a turbine, made with UV-transparent polymer, keeps it in turbulent motion. The possibility to rotate the turbine at controlled speeds allows to reduce the diffusion limit layer above the catalytic surface, as previously described in the model. The key points of this photoreactor are the strong versatility and maneuverability due to its small size, that allow also a great measurement speed.

RESULTS AND DISCUSSION

Spectroscopic characterization. The alteration of the ionic charge caused by the presence of an aliovalent element into an ionic lattice is a well-known phenomenon in solid-state chemistry. In the case of titanium dioxide, the introduction of F^- ions in the oxide matrix during the synthesis, leads to the formation of Ti^{3+} ions revealed by characteristic EPR and UV-Vis spectra.[17, 27-28] The concentration of F^- (and of their Ti^{3+} counterpart) in the solid can be tuned using different preparation methods. In particular, in the present work high doping levels are achieved via a hydrothermal synthesis leading to highly fluorinated, blue coloured, TiO_2 nanosheets exposing {001} facets. To clarify the impact on the electronic properties of the TiO_2 NPs induced by the processes employed to remove F^- from the surface (i.e. anion exchange in NaOH solution, sample named n-sh_NaOH) and from the bulk (i.e. calcination at 873 K, sample named n-sh_873K), the samples were investigated by UV-Vis-NIR-MIR and CW and pulse EPR spectroscopies. In Figure 1, we show the diffuse reflectance UV-Vis-NIR-MIR spectra of the pristine (n-sh), ion exchanged (n-sh_NaOH) and calcined (n-sh_873K) TiO_2 nanoparticles. The spectrum of the pristine sample shows a very broad absorption covering all the 15000-4000 cm^{-1} (660-2500 nm) range, due to trapped excess electrons resulting from the substitution of O^{2-} ions by F^- ions.[17, 29] The spectral profile of this sample shows a continuous increase in absorbance also in the MIR region (Figure 1, right part) typical of free conduction band and shallow-trapped electrons.[30-33] In the MIR spectra we see also a broad band in the 3600-2800 cm^{-1} range, vibrational in nature, which can be assigned to the stretching vibration ν(OH) of hydrogen bonded hydroxyls and water molecules, adsorbed on the surface of the nanoparticles.[34-36]

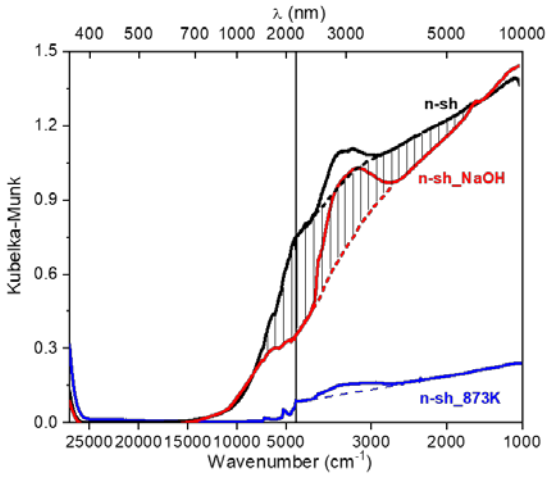

Figure 1. Diffuse reflectance UV-Vis-NIR (left) and MIR (right) spectra of the three different TiO_2 samples. The spectra in the MIR region have been vertically translated to align them with the spectra in the NIR region. The dashed lines highlight the TiO_2 spectral profile in the region (3600-2800 cm^{-1}) in which vibrational signals due to adsorbed surface species are present. The vertical black lines highlight the difference in absorption between the n-sh and n-sh_NaOH samples.

As discussed in detail in our previous publication,[22] the intensity of the ν(OH) band varies in agreement with the different surface hydration/hydroxylation of the samples arising from the different post-synthesis treatments. Moving to the sample treated with NaOH, the electronic absorptions are similar to the pristine sample, although lower in intensity in the NIR spectral region. The area highlighted by the vertical lines in Figure 1 represents the difference in absorption between the n-sh and n-sh_NaOH samples, which shows a broad maximum around 4000 cm^{-1} and can be interpreted as the absorption associated to the surface Ti^{3+} species. Indeed, this reduction of the absorption is compatible with the elimination of the F^- (and the associated Ti^{3+} species) from the (sub-)surface layer of the nanoparticles, while the bulk still contains a large concentration of Ti^{3+} ions.[33] This interpretation, involving a (sub-)surface oxidation promoted by NaOH to obtain stoichiometric TiO_2, is also supported by the EPR results (*vide infra*). Finally, the calcination process leads to the complete disappearance, in the whole 15000-1000 cm^{-1} range, of the spectral features ascribed to electronic defects associated with the presence of F^-, suggesting that fluorine has been completely removed, in agreement with previous XPS and TOF-SIMS measurements.[22]

Further insights into the nature of the Ti^{3+} ions generated in the solid by the introduction of F^- are given by EPR spectroscopy. After high vacuum treatments at 373 K (residual pressure $<10^{-3}$ mbar) to remove surface adsorbates, the as prepared F-TiO_2 samples display EPR spectra (Figure 2) characterized by a powder-like axial pattern with $g_{zz} = g_{\parallel} = 1.962$ and $g_{xx} = g_{yy} = g_{\perp} = 1.992$, in

line with typical F-doped TiO_2 systems,[19, 37] although displaying unusually broad line widths, likely associated to dipole-dipole broadening and indicating a large concentration of Ti^{3+} species. This is consistent with the absence of an electron spin echo signal for sample n-sh and detection of only a weak echo signal for sample n-sh-NaOH, due to fast phase memory time (T_m< 90 ns the spectrometer dead time). Quantitative evaluations indicate a Ti^{3+} concentration of the order of 1.14 x 10^{18} spin/g. In the case of F-TiO_2 prepared by wet chemistry methods, it is crucial to discriminate between the possible formation of both surface and bulk F^- dopants and the correlated Ti^{3+} surface and bulk states. Clearly surface states will deeply affect the chemistry at the solid/adsorbate interface, while bulk impurities will alter the electronic structure of the solid, both situations impacting, in different ways, on the chemical reactivity of the modified solid. The insertion of fluorine in the TiO_2 matrix has been demonstrated to generate localized electrons in the t_2g orbitals of the Ti cations without generating oxygen vacancies. On the other hand, surface diamagnetic F_{surf}-TiO_2 centers have been identified by the X-ray photoemission spectroscopy technique (XPS).[17] However, no clear evidence of surface Ti^{3+} ions has been obtained so far for F doped TiO_2 samples.[37]

Reduced titanium species localized at the surface are characterized by distinctive broad EPR spectra, which are best observed by means of electron spin echo (ESE) detected EPR experiments.[27] The ESE-detected EPR spectrum corresponds to the absorption of the conventional CW-EPR spectrum and is more effective in detecting broad signals, which become hardly observed in conventional CW-EPR experiments, which provide the absorption derivative. The ESE detected EPR spectrum of the pristine sample, under high vacuum, is reported in Figure 3 and clearly shows the presence of a broad absorption, indicated with OP1, centred approximately at g=1.93 (B_0 = 380 mT). This broad signal, hardly detectable, even at high modulation amplitudes, in conventional CW EPR experiments, has been assigned to a collection of surface and subsurface reduced Ti^{3+} centers whose heterogeneity derives from several factors including the local coordination of the ion, the symmetry of the particular crystal face hosting the reduced ion, and the presence of magnetically active nuclei located in the vicinity of the paramagnetic centres. In our case magnetically active nuclei are associated to surface F ions, whose presence can be revealed by means of Electron Spin Echo Envelope Modulation (ESEEM) experiments. Two-pulse ESEEM (2P-ESEEM) spectra were then taken at magnetic field settings corresponding to the maximum absorption of bulk Ti^{3+} and of the broad resonance at g=1.93 (indicated by the arrows in Figure 3), respectively.

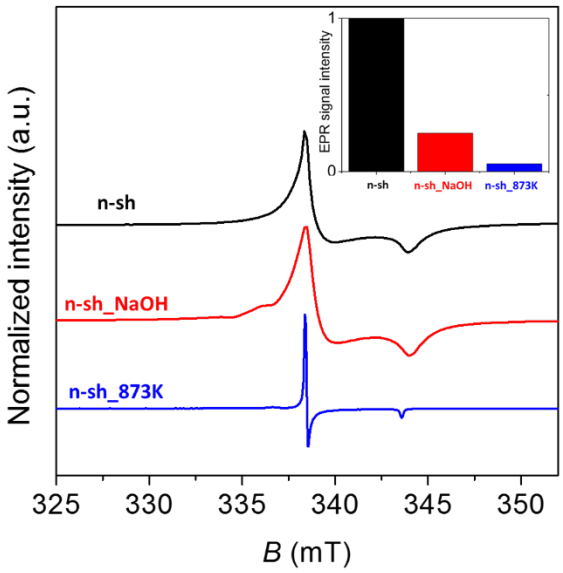

Figure 2. X-band CW EPR spectra of the three different TiO_2 samples recorded at 77 K. All samples were treated under high vacuum at 373 K.

The 2P-ESEEM spectrum (Figure 3a) recorded at a magnetic field position corresponding to the maximum of the broad absorption of the echo signal (OP1 in Figure 3) shows clear ^{19}F modulations, which are absent in the spectrum (Figure 3c) recorded at a magnetic field corresponding to the narrow ESE line (OP2). The corresponding Fourier transform are shown in Figure 3b,d. This observation provides compelling evidence that the two different Ti^{3+} species are characterized by a different local environment. In particular, despite the low echo intensity of the broad species, the ^{19}F modulations are clearly visible, indicating a high number of ^{19}F nuclei interacting with the Ti^{3+} centres, a clear proof of the surface nature of these species, characterized by a ^{19}F rich environment. On the contrary, the 2P-ESEEM pattern recorded at field positions corresponding to the narrow feature of the Ti^{3+} species, does not show such modulations, confirming the bulk nature of this species as already observed in the past by means of ^{17}O ESEEM experiments.[20] Further evidence of the surface nature of the Ti^{3+} species is obtained by performing the same experiment after washing the sample with a NaOH solution (0.1 M). This treatment removes surface F^- ions oxidizing the associated Ti^{3+} species to diamagnetic Ti^{4+} ions. As a result, the spectral intensity is decreased to approximately 25 % of the initial value (inset in Figure 2), with a strong depletion of the broad absorption feature (Figure 3b).

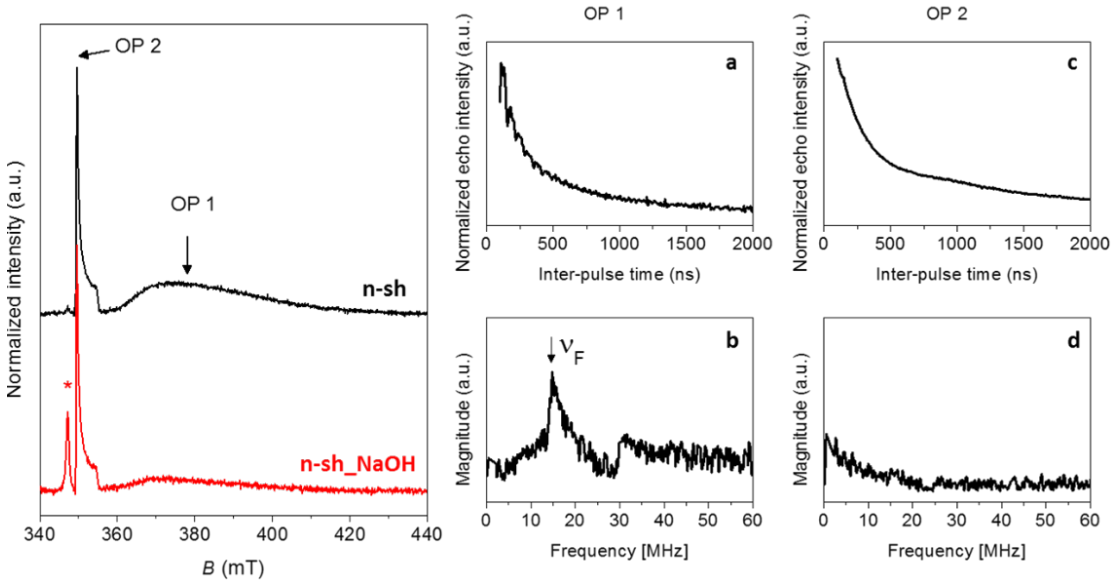

Figure 3. ESE-detected EPR spectra of n-sh and n-sh_NaOH. 2P-EESEEM spectra of n-sh, taken at OP1 (a) and OP2 (c) and their corresponding Fourier transform (b,d). All of the spectra were recorded at T = 10 K.

Finally, calcination of the sample at high temperature leads to a strong depletion of the Ti^{3+} centres, which are reduced to approximately 5% of the initial value (inset in Figure 2) and diluted in the diamagnetic host matrix as reflected by the drastic decrease of the spectral line width. This trend correlates with the total number of F^- ions present in the sample, as determined by ion chromatography, although the number of F^- ions is found to systematically exceed the number of EPR active Ti^{3+} species. Pristine TiO_2 n-sh is found to contain 16±1 mg F^-/g TiO_2, decreasing to 7±1 mg F^-/g TiO_2 for the_NaOH treated sample (n-sh_NaOH) and less than 0.4 mg F^-/g TiO_2 for the calcined sample. The reason for the discrepancy between the number of Ti^{3+} species detected by EPR and the overall F content (approximately 1:500), can be explained considering that only a fraction of the F^- ions enters the TiO_2 structure leading to a valence induction mechanism. Moreover, we remark that an underestimation of the EPR active Ti^{3+} species related to signal OP1 is very likely, due to the broad line-width of the signal.

In summary, combined CW and pulse EPR experiments indicate that the F-TiO_2 sample exhibits both terminating surface Ti^{3+} centres and bulk Ti^{3+} due to F-doping during the synthesis. The surface Ti^{3+} species are characterized by a broad EPR spectrum and the proximity of F^- ions. These surface species are progressively reduced by washing treatments with NaOH, which deplete the surface fluorides responsible for the Ti^{3+} stabilization, leaving a OH^- terminated surface. Further, high temperature thermal treatments, strongly reduce the number of bulk F^- ions as reflected by the drastic decrease of the bulk Ti^{3+} signal.

Dynamics of the photogenerated charge carries. To investigate the impact of post-synthesis treatments on the carriers behavior of the three TiO_2 materials discussed so far (i.e. F^- terminated, OH^- terminated and bare (1×4) reconstructed {001} TiO_2 NPs), light-induced EPR (also in presence of molecular scavengers) and photoelectrochemical experiments were carried out. These techniques allow investigating the kinetics of surface transfer or recombination of the photogenerated charge carriers. These complementary methods interrogate the nanoparticles from two different point of view and in two different environments (gas-solid and liquid-solid interfaces), but the final results, although not quantitatively comparable, can lead to a critical evaluation of the impact on the (photo-) chemical reactivity induced by post-synthesis treatments. To test the photochemical reactivity towards electron and hole transfer at gas-solid interface, EPR experiments were carried out under UV irradiation in vacuum and in the presence of O_2 and H_2, which act as electron and hole scavengers respectively (Figure 4). Irradiation under vacuum with above band gap energies is expected to generate paramagnetic charge separated states, which can be described in chemical terms as Ti^{3+} and O^- transient species. After 10 min of UV illumination under vacuum at 77 K of the as prepared sample, we observe the appearance of weak EPR signals, partially overlapping with the Ti^{3+} signal, at $g > g_e$ and g values typical of surface O^- species (g_1=2.026 g_2=2.014 g_3=2.003) formed by hole trapping at surface O^{2-} sites.[37-39] Irradiation of the same sample under O_2 (an electron scavenger) or H_2 (a hole scavenger) atmosphere, leads to similar EPR spectra (Figure 4). The absence of the typical EPR signal due to superoxo radical species upon photo-irradiation of the sample under oxygen, may suggest that the surface

fluorinated sample with exposed {001} facets is either unable to stabilize such paramagnetic species or features a reduced interfacial charge transfer capability. Indeed, fluorides are able to stabilize electrons, by lowering the position of the band edges in anatase, thus reducing their interfacial transfer, in particular towards reaction with O_2.[37, 40] A different situation is observed upon removal of the fluorinated surface by means of NaOH washing. Under these circumstances UV irradiation under vacuum induces minor changes in the original EPR spectrum (Figure 4). After irradiation under H_2, the intensity of the Ti^{3+} signal increases of a factor of 3. This result indicates that surface holes are formed, which react with H_2 according to the following reactions as already observed by Diwald et al.: [41]

$$2O^{2-}_{surf} + h^+ + H_2 \rightarrow OH^-_{surf} + O^{2-}_{surf} + H$$

$$OH^-_{surf} + O^{2-}_{surf} + H \rightarrow 2OH^-_{surf} + e^-$$

The complementary experiment involving O_2 as an electron scavenger, leads to the appearance of a new signal characterized by $g_{\|}$ = 2.036 and $g_{\perp}$ = 2.005, which is assigned to surface adsorbed superoxide ions, formed via a direct surface to molecule electron transfer, according to the following reaction:

$$Ti^{3+}_{surf} + O_2 \rightarrow Ti^{4+} + O_2^-(surface)$$

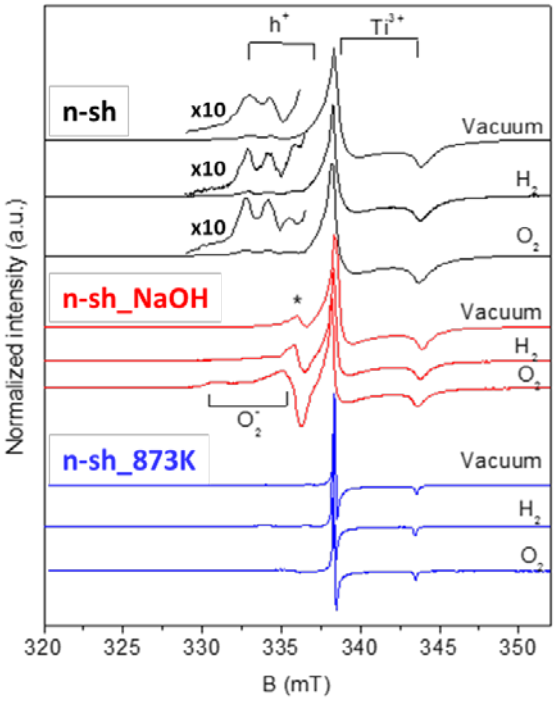

Figure 4. CW-EPR spectra of n-sh, n-sh_NaOH and n-sh_873K, recorded in dark upon 10 minutes' irradiation in vacuum, in H_2 and in O_2. All of the spectra were recorded at T = 77 K. h^+ indicates the spectral region where hole signals are found. The asterisk indicates an irreproducible signal at g = 2.005 whose nature is unassigned.

The intensity of the superoxide signal corresponds thus to the fraction of surface reactive Ti^{3+} species generated under irradiation. Quantitative evaluation of the EPR spectra obtained upon irradiation under H_2 and O_2 indicates that the fraction of chemically reactive surface hole centres generated under irradiation is slightly higher (approximately 1.7 times) than that of the surface Ti^{3+} centres, suggesting a moderately higher oxidative capacity of the sample (Figure 4). Finally, we notice that the reactivity of the calcined samples is strongly inhibited, and no significant spectral change are observed upon UV illumination under the above reported conditions.

Considering that TiO_2 nanoparticles are widely used as photocatalyst also in aqueous media, electrochemical experiments are a relevant tool to investigate the dynamic of the charge carriers' recombination in a different environment respect to EPR measurements. The recombination rate constant for electrons and holes generated upon illumination of the studied TiO_2 nanoparticles can be studied by means of electrochemical measurements on TiO_2 electrodes.[21] Measurements are based on a combination of cyclic voltammetry (CV) and open circuit photopotential (OCP) relaxation tests. In this way, it is possible to obtain the density of charge carriers generated and their recombination rate.

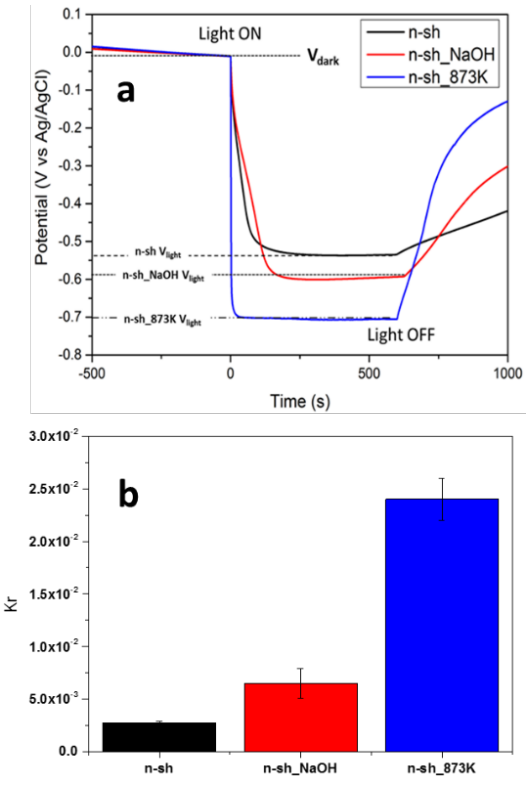

Figure 5. OCP (a) and recombination rate Kr (b) of the three considered materials under N_2 atmosphere under an UV irradiation (365 nm) of 20 W m^{-2}. Kr considered until $4.0*10^{16}$ charge carriers' density.

As mentioned, the fluorination of the TiO_2 nanoparticles can change the recombination rate of the photogenerated electrons and holes and the carrier transfer to solution. The OCP measurements carried out under a N_2 atmosphere can be used to evaluated the effect of morphology and fluorides on the charge carrier recombination in the semiconductor and on the ability of the materials to accumulate electrons. Indeed, the photopotential obtained results from the balance between electrons accumulation and recombination. Photo-holes are readily injected in solution across the space charge layer in this n-type semiconductor. If the rate of the recombination process is lower than the electrons accumulation rate, the result is a net storage of electrons that makes the photo-potential more negative. From the decay of the photopotential, the recombination rate constants (k_r) can be calculated (Figure 5). Figure 5a highlights that the decreased fluorides doping leads to higher photo-potential ($\Delta V = V_{light}-V_{dark}$), confirming the stabilization of Ti^{3+} sites by fluorides (photopotential less negative). The photo-potential obtained for n-sh_873K is higher than for the fluorinated materials, and with an apparent increased recombination rate. While the recombination rate is very low for the material n-sh comparing to the others, due to the stabilizing effect of fluorides at the surface. The higher k_r obtained for the material n-sh_873K (Figure 5b) is due to the low stabilization of the carriers associated to the almost complete removal of the fluorides and the extremely poor surface hydroxylation.[22] Moreover, the lack of trap surface states induces a great bulk recombination and, therefore, a weak interfacial charge transfer in agreement with the EPR results.

Photocatalytic Degradation of Nitric Oxide. The photocatalytic activity of the three studied materials were evaluated monitoring the abatement of the nitric oxide. The tests were carried out in a previously developed gas/solid photoreactor.[26] The materials were tested under four different UV irradiances (10, 22, 48 and 83 W m^{-2} with LED centred at 360nm) and four different initial NO concentration (0.5, 1.1, 2.2 and 4.2 ppmv). The dependence of substrate disappearance rate on its concentration has a saturative behaviour and a square root dependence on the irradiance. These behaviours are the result of the balance between recombination and interfacial charge transfer rates in the limits of high irradiances (relatively photogenerated carrier concentrations) or high substrate concentration (high availability of substrate at the surface), the process that controls the disappearance rate of the substrate is related to the interfacial charge transfer rate.[42-43] Figure 6 shows that at low NO initial concentration or low irradiances the differences between the materials are less relevant. With the increase of the NO initial concentration the differences become apparent. If the fluorides are removed only from the surface of the nanoparticles (n-sh_NaOH) an increase of the activity is obtained, conversely the calcination at 873K (n-sh_873K) largely decrease the activity.

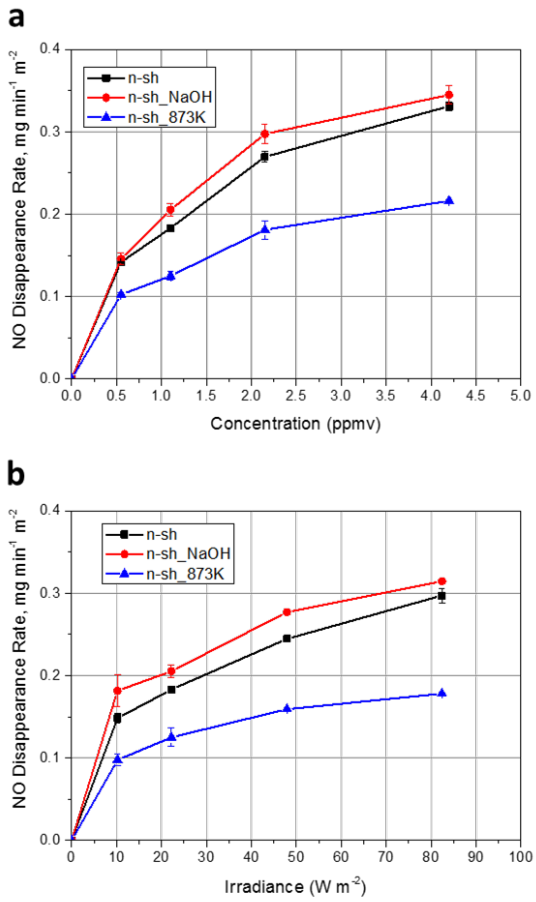

Figure 6. Dependence of the NO disappearance rates from the NO initial concentration (a) and from the irradiance (b) on the TiO_2 films.

The nanosheets calcination drastically reduces the photoactivity, whereas the treatment with NaOH slightly increase the NO degradation. These behaviours can be ascribed to two main aspects: the first is the change of the surface hydrophilicity that could increase or decrease the interaction with water of the material's surface, as described in a previous work also in the material here analysed.[22] The second aspect is the one described in this work, i.e. the post-synthesis treatments are able to modify the electronic properties of the materials, changing the ability of their charge carriers to be transferred to the surface (and react with oxidants and reducing agents) or recombine.

CONCLUSIONS

In conclusion, the work presents the effect of two different post-synthesis treatments on the electronic properties, and consequently on the photoactivity, of shape controlled TiO_2 nanoparticles that largely expose formally {001} facets. The electronic characterization, carried out by UV-Vis-NIR-MIR and CW-EPR spectroscopies,

highlights the effect of the two different treatments in the fluorides removal from the nanoparticles. The NaOH washing method is limited to the surface, while, the thermal treatment at 873K impacts on the bulk of the TiO_2 NPs. In the case of F-TiO_2 prepared by wet chemistry methods, it is crucial to discriminate between the possible formation of both surface and bulk F^- dopants and the correlated Ti^{3+} surface and bulk states and their fate upon different post-synthesis treatments. Pulsed EPR experiments allowed to discriminate between surface and bulk Ti^{3+}states, evidencing the presence of stable surface Ti^{3+} species with a F^- rich environment. These species are strongly depleted by NaOH treatments as a consequence of the removal of surface fluorides. Such treatments lead to OH^- terminated {001} surfaces[8] with a strong influence on the dynamic of photo-generated charge carriers, and on the reactivity of the material. CW-EPR measurements under irradiation under three different atmospheres (vacuum, hydrogen and oxygen) demonstrate that the surface reactivity at the gas/solid interface is significantly altered depending on the specific post-synthesis treatment. Removal of surface fluorides results in an increase of the photoelectron interfacial transfer as probed by the formation of superoxo radical anions upon UV irradiation in the presence of molecular oxygen as an electron scavenger. This effect can be explained considering the stabilization of Ti^{3+} by F^- ligands.[44-45] The thermal treatment, on the other hand, leads to a complete inhibition of the surface reactivity of the material. This is probably due to the (1×4) reconstruction of {001} surfaces as reported by Mino et al.[22] that can reduce the interfacial transfer of both electrons and holes. The combination of these two effect results in a higher recombination rate of the carriers in the bulk of the material. To prove this, electrochemical measurements were carried out in an aqueous environment to evaluate the effect of fluorides on the charge carriers' density and their recombination kinetics. As expected, the general effect is a decrease of the recombination rate (in absence of any scavenger) due to the surface electron traps (Ti^{3+}) stabilization. The removal of the surface fluorides, slightly increases the recombination rate (k_r) of the charge carrier, but as seen from the EPR experiments under irradiation, largely increases the interfacial transfer of the photogenerated electrons and holes. TiO_2 NPs treated at 873K are characterized by a very high charge carriers' recombination rate due to the absence of surface trap states capable to stabilize the photogenerated charge carriers, decreasing interfacial charge transfer rates in synergy with the extended differences in surface structure and hydration.

Supporting Information. Supporting Information contain details about the electrochemical and photocatalytic measurements.

AUTHOR INFORMATION

Corresponding Author

*E-mail: mario.chiesa@unito.it;

Author Contributions

The manuscript was written through contributions of all authors. All authors have given approval to the final version of the manuscript.

Funding Sources

The authors acknowledge funding from:

- SETNanoMetro, EU Project, FP7-NMP-2013_LARGE-7. Project number: 604577;
- Regione Piemonte, Bando LR34/2004 — "Studio preliminare e sviluppo di soluzioni innovative di materiali d'attrito in ambito Automotive";

REFERENCES

1. Liu, G.; Yu, J. C.; Lu, G. Q.; Cheng, H. M., Crystal Facet Engineering of Semiconductor Photocatalysts: Motivations, Advances and Unique Properties. *Chem. Commun.* **2011**, *47*, 6763-6783.
2. Kamat, P. V., Semiconductor Surface Chemistry as Holy Grail in Photocatalysis and Photovoltaics. *Accounts of chemical research* **2017**, *50*, 527-531.
3. Yang, H. G.; Sun, C. H.; Qiao, S. Z.; Zou, J.; Liu, G.; Smith, S. C.; Cheng, H. M.; Lu, G. Q., Anatase Tio2 Single Crystals with a Large Percentage of Reactive Facets. *Nature* **2008**, *453*, 638-41.
4. Ong, W. J.; Tan, L. L.; Chai, S. P.; Yong, S. T.; Mohamed, A. R., Highly Reactive {001} Facets of Tio2-Based Composites: Synthesis, Formation Mechanism and Characterization. *Nanoscale* **2014**, *6*, 1946-2008.
5. Yang, X. H.; Li, Z.; Sun, C.; Yang, H. G.; Li, C., Hydrothermal Stability of {001} Faceted Anatase Tio2. *Chemistry of Materials* **2011**, *23*, 3486-3494.
6. Liu, S.; Yu, J.; Jaroniec, M., Anatase Tio2with Dominant High-Energy {001} Facets: Synthesis, Properties, and Applications. *Chemistry of Materials* **2011**, *23*, 4085-4093.
7. Ohno, T.; Sarukawa, K.; Matsumura, M., Crystal Faces of Rutile and Anatase Tio2 Particles and Their Roles in Photocatalytic Reactions. *New Journal of Chemistry* **2002**, *26*, 1167-1170.
8. Bae, E.; Murakami, N.; Ohno, T., Exposed Crystal Surface-Controlled Tio2 Nanorods Having Rutile Phase from Ticl3 under Hydrothermal Conditions. *Journal of Molecular Catalysis A: Chemical* **2009**, *300*, 72-79.
9. Bae, E.; Ohno, T., Exposed Crystal Surface-Controlled Rutile Tio2 Nanorods Prepared by Hydrothermal Treatment in the Presence of Poly(Vinyl Pyrrolidone). *Applied Catalysis B: Environmental* **2009**, *91*, 634-639.
10. Murakami, N.; Kurihara, Y.; Tsubota, T.; Ohno, T., Shape-Controlled Anatase Titanium(Iv) Oxide Particles Prepared by Hydrothermal Treatment of Peroxo Titanic Acid in the Presence of Polyvinyl Alcohol. *The Journal of Physical Chemistry C* **2009**, *113*, 3062-3069.
11. D'Arienzo, M.; Carbajo, J.; Bahamonde, A.; Crippa, M.; Polizzi, S.; Scotti, R.; Wahba, L.; Morazzoni, F., Photogenerated Defects in Shape-Controlled Tio2 Anatase Nanocrystals: A Probe to Evaluate the Role of Crystal Facets in Photocatalytic Processes. *J Am Chem Soc* **2011**, *133*, 17652-17661.
12. Di Liberto, G.; Tosoni, S.; Pacchioni, G., Role of Heterojunction in Charge Carrier Separation in Coexposed Anatase (001)-(101) Surfaces. *The journal of physical chemistry letters* **2019**, *10*, 2372-2377.

13. Pellegrino, F.; Sordello, F.; Mino, L.; Minero, C.; Hodoroaba, V.-D.; Martra, G.; Maurino, V., Formic Acid Photoreforming for Hydrogen Production on Shape-Controlled Anatase Tio2 Nanoparticles: Assessment of the Role of Fluorides, {101}/{001} Surfaces Ratio, and Platinization. *ACS Catalysis* **2019**, 6692-6697.
14. Pellegrino, F.; Sordello, F.; Minella, M.; Minero, C.; Maurino, V., The Role of Surface Texture on the Photocatalytic H2 Production on Tio2. *Catalysts* **2019**, *9*, 32.
15. Asahi, R.; Morikawa, T.; Irie, H.; Ohwaki, T., Nitrogen-Doped Titanium Dioxide as Visible-Light-Sensitive Photocatalyst: Designs, Developments, and Prospects. *Chemical reviews* **2014**, *114*, 9824-52.
16. Livraghi, S.; Paganini, M. C.; Giamello, E.; Selloni, A.; Di Valentin, C.; Pacchioni, G., Origin of Photoactivity of Nitrogen-Doped Titanium Dioxide under Visible Light. *J Am Chem Soc* **2006**, *128*, 15666-71.
17. Czoska, A. M.; Livraghi, S.; Chiesa, M.; Giamello, E.; Agnoli, S.; Granozzi, G.; Finazzi, E.; Di Valentin, C.; Pacchioni, G., The Nature of Defects in Fluorine-Doped Tio_2. *J. Phys. Chem. C* **2008**, *112*, 8951-8956.
18. Herrmann, M.; Kaluza, U.; Boehm, H. P., Über Die Chemie Der Oberfläche Des Titandioxids. Iv. Austausch Von Hydroxidionen Gegen Fluoridionen. *Z. Anorg. Allg. Chem.* **1970**, *372*, 308-313.
19. Minero, C.; Mariella, G.; Maurino, V.; Pelizzetti, E., Photocatalytic Transformation of Organic Compounds in the Presence of Inorganic Anions. 1. Hydroxyl-Mediated and Direct Electron-Transfer Reactions of Phenol on a Titanium Dioxide-Fluoride System. *Langmuir* **2000**, *16*, 2632-2641.
20. Minero, C.; Bedini, A.; Maurino, V., Glycerol as a Probe Molecule to Uncover Oxidation Mechanism in Photocatalysis. *Appl. Catal. B-Environ.* **2012**, *128*, 135-143.
21. Monllor-Satoca, D.; Gomez, R., Electrochemical Method for Studying the Kinetics of Electron Recombination and Transfer Reactions in Heterogeneous Photocatalysis: The Effect of Fluorination on Tio2 Nanoporous Layers. *J. Phys. Chem. C* **2008**, *112*, 139-147.
22. Mino, L.; Pellegrino, F.; Rades, S.; Radnik, J.; Hodoroaba, V.-D.; Spoto, G.; Maurino, V.; Martra, G., Beyond Shape Engineering of Tio_2 Nanoparticles: Post-Synthesis Treatment Dependence of Surface Hydration, Hydroxylation, Lewis Acidity and Photocatalytic Activity of Tio_2 Anatase Nanoparticles with Dominant {001} or {101} Facets. *ACS Appl. Nano Mater.* **2018**, *1*, 5355-5365.
23. Han, X.; Kuang, Q.; Jin, M.; Xie, Z.; Zheng, L., Synthesis of Titania Nanosheets with a High Percentage of Exposed (001) Facets and Related Photocatalytic Properties. *J Am Chem Soc* **2009**, *131*, 3152-3.
24. Zhang, J.; Wang, J.; Zhao, Z.; Yu, T.; Feng, J.; Yuan, Y.; Tang, Z.; Liu, Y.; Li, Z.; Zou, Z., Reconstruction of the (001) Surface of Tio2 Nanosheets Induced by the Fluorine-Surfactant Removal Process under Uv-Irradiation for Dye-Sensitized Solar Cells. *Phys Chem Chem Phys* **2012**, *14*, 4763-9.
25. Maurino, V.; Minero, C.; Pellegrino, F.; Zangirolami, M. System for Lighting and Measuring the Photo-Catalytic Activity of the Reactive Surface of a Material. 19-05-2017, 2017.
26. Pellegrino, F.; Zangirolami, M.; Minero, C.; Maurino, V., Portable Photoreactor for on-Site Measurement of the Activity of Photocatalytic Surfaces. *Catalysis Today* **2020**, *340*, 363-368.
27. Livraghi, S.; Chiesa, M.; Paganini, M. C.; Giamello, E., On the Nature of Reduced States in Titanium Dioxide as Monitored by Electron Paramagnetic Resonance. I: The Anatase Case. *J. Phys. Chem. C* **2011**, *115*, 25413–25421.
28. Jain, S. M.; Biedrzycki, J. J.; Maurino, V.; Zecchina, A.; Mino, L.; Spoto, G., Acetylene Oligomerization on the Surface of Tio2: A Step Forward in the in Situ Synthesis of Nanostructured Carbonaceous Structures on the Surface of Photoactive Oxides. *J. Mater. Chem. A* **2014**, *2*, 12247-12254.
29. Di Valentin, C.; Pacchioni, G.; Selloni, A., Reduced and N-Type Doped Tio_2: Nature of Ti^{3+} Species. *J. Phys. Chem. C* **2009**, *113*, 20543-20552.
30. Panayotov, D. A.; Burrows, S. P.; Morris, J. R., Infrared Spectroscopic Studies of Conduction Band and Trapped Electrons in Uv-Photoexcited, H-Atom N-Doped, and Thermally Reduced Tio_2. *J. Phys. Chem. C* **2012**, *116*, 4535-4544.
31. Gordon, T. R.; Cargnello, M.; Paik, T.; Mangolini, F.; Weber, R. T.; Fornasiero, P.; Murray, C. B., Nonaqueous Synthesis of Tio2 Nanocrystals Using Tif4 to Engineer Morphology, Oxygen Vacancy Concentration, and Photocatalytic Activity. *J Am Chem Soc* **2012**, *134*, 6751-6761.
32. Mino, L.; Zecchina, A.; Martra, G.; Rossi, A. M.; Spoto, G., A Surface Science Approach to Tio_2 P25 Photocatalysis: An in Situ Ftir Study of Phenol Photodegradation at Controlled Water Coverages from Sub-Monolayer to Multilayer. *Appl. Catal. B-Environ.* **2016**, *196*, 135-141.
33. Barzan, C.; Mino, L.; Morra, E.; Groppo, E.; Chiesa, M.; Spoto, G., Photoinduced Ethylene Polymerization on Titania Nanoparticles. *ChemCatChem* **2017**, *9*, 4324-4327.
34. Deiana, C.; Fois, E.; Coluccia, S.; Martra, G., Surface Structure of Tio_2 P25 Nanoparticles: Infrared Study of Hydroxy Groups on Coordinative Defect Sites. *J. Phys. Chem. C* **2010**, *114*, 21531-21538.
35. Mino, L.; Spoto, G.; Bordiga, S.; Zecchina, A., Particles Morphology and Surface Properties as Investigated by Hrtem, Ftir, and Periodic Dft Calculations: From Pyrogenic Tio_2 (P25) to Nanoanatase. *J. Phys. Chem. C* **2012**, *116*, 17008-17018.
36. Mino, L.; Spoto, G.; Bordiga, S.; Zecchina, A., Rutile Surface Properties Beyond the Single Crystal Approach: New Insights from the Experimental Investigation of Different Polycrystalline Samples and Periodic Dft Calculations. *J. Phys. Chem. C* **2013**, *117*, 11186-11196.
37. Kus, M., et al., Mechanistic Insight into the Photocatalytic Working of Fluorinated Anatase {001} Nanosheets. *The Journal of Physical Chemistry C* **2017**, *121*, 26275-26286.
38. Chiesa, M.; Paganini, M. C.; Livraghi, S.; Giamello, E., Charge Trapping in Tio2 Polymorphs as Seen by Electron Paramagnetic Resonance Spectroscopy. *Phys Chem Chem Phys* **2013**, *15*, 9435-9447.
39. Micic, O. I.; Zhang, Y.; Cromack, K. R.; Trifunac, A. D.; Thurnauer, M. C., Trapped Holes on Titania Colloids Studied by Electron Paramagnetic Resonance. *The Journal of Physical Chemistry* **1993**, *97*, 7277-7283.
40. Monllor-Satoca, D.; Lana-Villarreal, T.; Gomez, R., Effect of Surface Fluorination on the Electrochemical and Photoelectrocatalytic Properties of Nanoporous Titanium Dioxide Electrodes. *Langmuir* **2011**, *27*, 15312-21.
41. Berger, T.; Diwald, O.; Knözinger, E.; Napoli, F.; Chiesa, M.; Giamello, E., Hydrogen Activation at Tio2 Anatase Nanocrystals. *Chemical Physics* **2007**, *339*, 138-145.
42. Emeline, A. V.; Ryabchuk, V. K.; Serpone, N., Dogmas and Misconceptions in Heterogeneous Photocatalysis. Some Enlightened Reflections. *The journal of physical chemistry. B* **2005**, *109*, 18515-21.
43. Minero, C., Kinetic Analysis of Photoinduced Reactions at the Water Semiconductor Interface. *Catalysis Today* **1999**, *54*, 205-216.
44. Blondel, C.; Delsart, C.; Goldfarb, F., Electron Spectrometry at the µev Level and the Electron Affinities of Si and F. *Journal of Physics B: Atomic, Molecular and Optical Physics* **2001**, *34*, L281-L288.
45. Goldfarb, F.; Drag, C.; Chaibi, W.; Kroger, S.; Blondel, C.; Delsart, C., Photodetachment Microscopy of the P, Q, and R Branches of the Oh(-)(V=0) to Oh(V=0) Detachment Threshold. *The Journal of chemical physics* **2005**, *122*, 14308.

TOC Graphic